

# Chapter 7

## Selection of GMI Wires for Sensor Applications

### 7.1 Criteria for Selecting GMI Materials

To search for a GMI material for GMI sensor applications, two main requirements should be satisfied, namely a high GMI ratio (or a large GMI effect) and a high sensitivity to the applied field (or a high magnetic response). In view of the theoretical analyses and experimental results, it is concluded that a large GMI effect should exist in magnetic materials with the following desirable properties:

- low resistivity,  $\rho$ ;
- high magnetic permeability,  $\mu$ ;
- high saturation magnetisation,  $M_s$ ; and
- small ferromagnetic relaxation parameter (or low damping parameter),  $\alpha$ .

In this context, crystalline ferromagnetic materials have the advantage of lower resistivity ( $\rho$ ), but amorphous ones have better soft magnetic behaviour (e.g. higher magnetic permeability,  $\mu$ , and saturation magnetisation,  $M_s$ ) because they lack magnetocrystalline anisotropy. In particular, non-magnetostrictive materials can be expected to show the best GMI performance because the magnetoelastic contribution to magnetic anisotropy substantially weakens the soft magnetic behaviour. Improvement in the magnetic softness of an actual amorphous material by appropriate thermal treatment and/or the application of external parameters (mechanical stress, magnetic field, etc.) can lead to a simultaneous improvement in the GMI effect and its field sensitivity. The damping parameter ( $\alpha$ ) is often considered in the high frequency range where ferromagnetic resonance takes place, while it can be neglected in the intermediate frequency range (i.e.  $f = 0.1\text{--}10$  MHz), where most GMI-based sensing applications have been identified (see Chap. 8). In addition, for practical sensor applications, the mass manufacturability and cost of materials are also important factors.

## 7.2 Evaluation of GMI Wires

In ferromagnetic materials, the highest value of the GMI effect experimentally observed is much smaller than the theoretically predicted value. Research in the field has been focused on special thermal treatments and on the development of new materials with properties appropriate for practical GMI sensor applications. In this section, all existing GMI wires will be reviewed and evaluated.

### 7.2.1 Co-Based Wires

Both conventional and glass-covered Co-based amorphous wires exhibit a GMI effect, owing to their high circular permeability. This is mainly due to the presence of circumferential anisotropy and an outer shell circular domain structure that results from coupling between negative magnetostriction and quenching compressive stress [1–5]. Among the Co-based amorphous alloys investigated, an alloy system with the nominal composition of Co–Fe–Si–B exhibits nearly zero and negative magnetostriction of  $\lambda_s = -0.4 \times 10^{-7}$ . This alloy is often obtained by alloying Fe–Si–B that has a positive  $\lambda_s$  of  $25 \times 10^{-6}$  with Co–Si–B that has a negative  $\lambda_s$  of  $-3 \times 10^{-6}$  [5, 6]. As a result, a record value of GMI ratio (1200 % at 14.2 MHz) has been achieved in the conventional amorphous  $\text{Co}_{68}\text{Fe}_{4.35}\text{Si}_{12.5}\text{B}_{15}$  wire [7]. This value is much larger than that reported earlier (600 %) with the same composition [2, 5]. This larger value of GMI ratio is a result of minimising contact resistance and cancelling parasitic impedance [7]. However, a high field sensitivity of GMI ( $\sim 500 \text{ %/Oe}$ ) was reported by Vazquez [2], while no information was found in the work by Garcia et al. [7].

In an attempt to develop magnetic wires for high-frequency sensor applications, Nie et al. [8] reported that a Co–Mn–Si–B amorphous glass-covered wire with nearly zero magnetostriction exhibited a GMI effect at high frequencies. For the amorphous  $\text{Co}_{68.2}\text{Mn}_7\text{Si}_{10}\text{B}_{15}$  microwire, the GMI ratio and magnetic response reached the values of 153 and 65 %/Oe, respectively, at a frequency of 30 MHz. Vinai et al. [9] recently revealed that these microwires also exhibited a GMI effect at frequencies up to GHz. In the frequency range of 100 MHz–6 GHz, the GMI ratio reached a maximum value of  $\sim 100 \text{ %}$  at a frequency of 2 GHz. As shown earlier in Chap. 6, for Co-based amorphous wires, the GMI effect can be further improved by appropriate field annealing [10], Joule current annealing [11–15], or the application of a tensile stress [16, 17].

In summary, the Co-based amorphous wires with nearly zero and negative magnetostriction are good candidates for GMI sensor applications. It should be noted that while the Co-based conventional and glass-covered amorphous wires are suitable for sensor applications in the low and intermediate frequency range (up to several MHz), the glass-covered amorphous microwires can be used for electrotechnical devices operating at much higher frequencies (up to several GHz). Due

to their relatively high resistivity, the microwires retain their large GMI value at higher frequencies, when compared to ribbons and wires. In practice, depending upon the specific requirements of a sensor device (e.g. the operating-frequency range), either wires or microwires should be chosen accordingly.

### 7.2.2 Fe-Based Wires

Fe-based amorphous wires have relatively small or even no MI effects, owing to their relatively small effective permeability, which is due to the presence of an outer shell radial domain configuration that results from the coupling between the highly positive magnetostriction and the quenching compressive stress [4, 10, 18, 19]. A primary alloy of Fe–Si–B having a positive  $\lambda_s$  of  $25 \times 10^{-6}$  was found to show poor magnetic softness and hence a small MI effect ( $\sim 3\%$ ), while a larger MI effect ( $\sim 36\%$ ) was obtained in the annealed wires [10, 19, 20]. It was the precipitation of an FeSi nanocrystalline phase that significantly decreased the bulk positive magnetostriction and hence gave rise to the MI effect of the annealed Fe–Si–B wires [20]. The crystallisation of Fe–Si–B-based amorphous alloys containing Nb and Cu causes the formation of a nanoscale bcc structure, and the bcc alloys exhibit excellent ultrasoft magnetic properties (i.e. high effective permeability and small coercivity) [6, 10]. In these alloys, the roles that Cu and Nb play are to maximise the density of crystal nuclei and to retard grain growth, respectively, leading to an ultrafine grain structure. Among these alloys, the nanocrystalline alloys with a nominal composition of  $\text{Fe}_{73.5}\text{Si}_{13.5}\text{B}_9\text{Nb}_3\text{Cu}_1$  were found to show the best magnetic softness. These materials are therefore expected to show large MI effects. Indeed, Knobel et al. [10] reported that conventional  $\text{Fe}_{73.5}\text{Si}_{13.5}\text{B}_9\text{Nb}_3\text{Cu}_1$  nanocrystalline wires (e.g. the amorphous wire samples annealed at 550–600 °C) exhibited a GMI effect. The largest value of GMI ratio was about 200 % at a frequency of 500 kHz for the wire sample annealed at 600 °C for 1 h. In another study, Li et al. [21] partially substituted Fe by Cr in  $\text{Fe}_{73.5}\text{Si}_{13.5}\text{B}_9\text{Nb}_3\text{Cu}_1$  nanocrystalline wires with the expectation of further reducing the magnetostriction of the primary alloy. They found that, although the GMI ratio and magnetic response were slightly smaller in Cr-doped samples, the addition of Cr improved the GMI response and significantly reduced the undesirable hysteretic effect in GMI curves with increasing and decreasing applied magnetic fields [21]. In addition, the presence of Cr significantly improved the corrosion resistance properties, which is desirable for sensing applications in a corrosive environment. The GMI effect was also observed in Fe-based nanocrystalline glass-coated wires and microwires [4, 18]. Interestingly, the  $\text{Fe}_{89}\text{B}_1\text{Si}_3\text{C}_3\text{Mn}_4$  nanocrystalline glass-covered microwires were found to show the GMI effect in the GHz frequency range [9]. At a frequency of 4 GHz, the GMI ratio reached a value as high as 70 % for the sample annealed at 350 °C. For this typical microwire, conventional furnace annealing proved more effective in improving the GMI effect compared with current annealing. Furthermore, it should be recalled that for both Fe-based amorphous

and nanocrystalline glass-covered wires, the removal of the glass layer can significantly improve the GMI effect and magnetic response. However, the GMI ratios of Fe-based nanocrystalline wires are often smaller than those of Co-based amorphous wires [5].

### 7.2.3 *Electrodeposited Wires*

Besides rapidly quenched wires, electrodeposited wires, which comprise a highly conductive non-magnetic metal core (e.g. Cu, CuBe, and Ag) and a thin layer of soft magnetic metal (e.g. NiFe, NiFeRu, NiFeMo, CoP, and CoNiFe), have been found to show excellent GMI behaviours [22–42]. For electrodeposited wires, the magnetic layer has either a circular or a radial domain configuration, depending strongly upon the alloy composition and the sample processing conditions [40]. Wires having a circular domain structure are often expected to show a larger MI effect [38, 42].

In a pioneering work, Usov et al. [38] predicted that the GMI effect could be further improved in a composite amorphous wire when the electrical conductivity of the inner core is much higher than that of the shell region. Since this work, experimental efforts have been devoted to investigating the GMI effect in electrodeposited wires, such as CoP/Cu [22–26, 39], NiFe/Cu [28–30, 41], CoNiFe/Cu [31, 32, 40], NiFeRu/Cu [33], and NiFeMo/Cu [34]. Sinnecker et al. [22] reported that an electrodeposited CoP/Cu wire exhibited radial magnetic anisotropy (i.e. the radial domain structure) and the size of the closure domains increased with the magnetic layer thickness (CoP). It is interesting to note that, although magnetic wires with a radial magnetic anisotropy are not expected to show any GMI effect, a significant increase in GMI ratio with the magnetic layer thickness of the CoP/Cu composite wire was attained [22]. This indicated that the observed GMI effect was associated with the current distribution along the sample radius, with two well-defined regions having different transport and magnetic properties [23–26]. Recently, Phan et al. [39] optimised the processing conditions in order to achieve the largest GMI effect in a typical CoP/Cu electrodeposited wire. The largest GMI ratio was achieved with a deposition time of 6 min and an electrolytic current density of 639 mA/cm<sup>2</sup>. At the measured frequency of 10.7 MHz, the GMI ratio and magnetic response reached the highest values of 534 and 21 %/Oe, respectively. It was proposed that the changes of deposition time and electrolytic current density caused variations in the domain structure of the CoP magnetic layer and hence the GMI behaviour [39]. More interestingly, Kurlyandskaya et al. [40] found that the GMI ratio reached a value as high as 1200 % at a frequency of 4 MHz for FeNiCo/CuBe electroplated wire. This is the highest value reported until now, among existing electrodeposited wires. However, no information on the magnetic response of GMI was given [40]. In a comprehensive study investigating the influences of processing parameters (e.g. electrodeposition current density, duty cycle, electrolyte solution, pH value, applied magnetic field, magnetic layers, and

post-annealing) on the GMI of electrodeposited NiFe/Cu wires, Li et al. [41] reported that the GMI ratio and magnetic response reached maximum values of 1110 and 218 %/Oe, respectively, at a frequency of 4 MHz for a dc Joule-annealed wire sample.

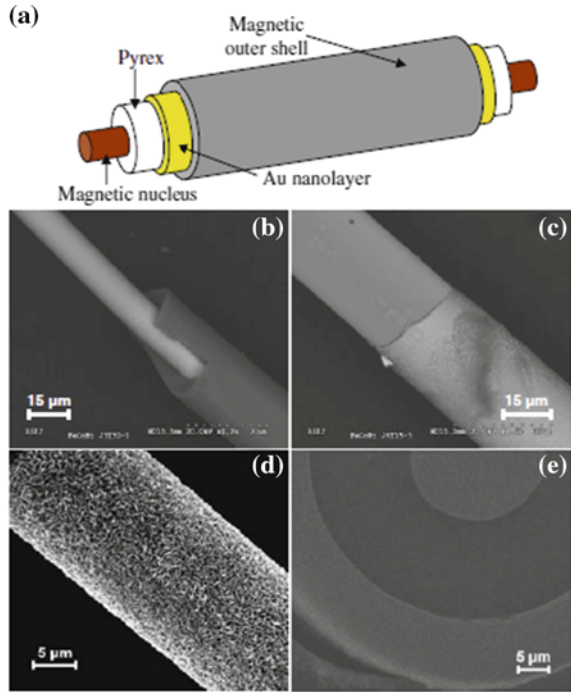
Recently, it has been revealed that the GMI effect can be further improved in electrodeposited wires by the inclusion of an insulating interlayer between the core and the magnetic shell (e.g. CuBe/insulator/NiFeB wires) [36, 37]. For instance, the GMI ratio reached a value of 250 % at  $f = 500\text{kHz} - 1\text{ MHz}$  for an electrodeposited CuBe/insulator/NiFeB wire, which is much larger than that of  $\sim 23\%$  at  $f = 1\text{ MHz}$  for the electrodeposited CuBe/NiFeB wire without the insulator layer [36]. This can arise from the differences in current distribution under the external magnetic field and from the electromagnetic interaction between the conductive core and the ferromagnetic layer of the composite wires with and without an insulator layer [36, 37]. In this context, Buznikov et al. [42] have recently developed a model for predicting the GMI effect in these typical wires. The model reveals that the field dependence of magnetic shell permeability significantly affects the eddy current distribution and therefore leads to the observed GMI effect. The inclusion of a thin insulator layer can lead to a further improvement in the GMI effect at sufficiently high frequencies, because it actually increases both the diagonal and off-diagonal impedance [42].

In general, electrodeposited composite wires are good candidate materials for producing high-performance magnetic sensors and sensing devices operating at low and intermediate frequencies (up to several MHz). Within this operating regime, electrodeposited composite wires may be even more promising than rapidly quenched wires and ribbons.

#### 7.2.4 *Multilayer Wires*

Multilayer wire is a new family of magnetic microwires with multilayer bimagnetic characteristics [43, 44]. A typical biphasic magnetic microwire consists of a ferromagnetic nucleus, an intermediate glass layer, and a ferromagnetic outer shell, as exemplified in Fig. 7.1. They were prepared by several complementary techniques including quenching and drawing for precursor glass-coated magnetic/metallic core microwire, sputtering for Au metallic intermediate nanolayer, and electroplating for magnetic external microtube. This combination of techniques enables the manipulation of different soft/hard magnetic characteristics at different layers and hence permits one to tune the properties of the biphasic microwires. The peculiarity of the multilayer wires lie in the coupling between various layers. The presence of an external magnetic shell around a glass-coated microwire induces a longitudinal anisotropy in the nucleus of the latter, drastically modifying its magnetoinductive behaviour, making it very sensitive to the presence of an applied external stress and temperature [45, 46].

**Fig. 7.1** **a** Scheme of multilayer microwire. SEM images of FeSiB/CoNi multilayer microwires: **b** FeSiB nucleus and glass cover, **c** glass layer and CoNi outer shell, **d** CoNi outer shell, and **e** cross-sectional view of the multilayer microstructure (reprinted with the permission of Springer [48])



The most notable magnetic characteristic is the step-like magnetisation process arising from the different magnetic phases and couplings [47]. These can be optimised by specific thermal treatment processing to grow a new structural phase with a hard magnetic character at the magnetic core via conventional thermal annealing, or by inducing suitable helical anisotropy at the magnetic shell via helical magnetic field annealing or torsion annealing. Different magnetic configurations have been explored thus far: soft (nucleus)/hard (outer shell), hard/soft, and soft/soft [48]. One can invariably make use of the magnetic interactions to manipulate the soft magnetic core behaviour. For instance, it can be modulated through the hard phase stray fields, or magnetic bistability can be modified through the magnetoelastic anisotropy induced by the external phase. In addition to the soft/hard magnetic nature of each magnetic phase, an effective tuning of average behaviour can be achieved by adapting the thickness of each layer.

These multilayer wires are of practical significance as sensing core elements in sensor devices. Subject to a delicate control in terms of the reversal magnetisation of the soft phase, this type of microwire has come to be an ideal candidate in a variety of sensor technologies from temperature/tensile stress and torsion/position sensors to coil-less orthogonal fluxgates. The versatility of their properties and the high degree of freedom for tailoring give these wires an outstanding edge in the competitive sensing technology field.

### 7.3 Nominated GMI Materials for Sensor Applications

A wide variety of GMI materials are currently available for practical GMI sensor applications. Table 7.1 summarises several materials that possess a high GMI ratio and magnetic response and are promising for making high-performance GMI sensors. Appropriate selection is dependent upon specific requirements, such as their field sensitivity, working frequency range, size, and thermal stability. The ultrahigh sensitivity of GMI to external dc magnetic field (down to  $10^{-8}$  Oe) can be used for magnetic field sensors and other sensors based on the change of a local magnetic field. It should be emphasised that not only the GMI ratio ( $\eta$ ) and the magnetic response ( $\zeta$ ), but also the particular shape of the  $\eta(H)$  curve are important

**Table 7.1** Candidate materials for GMI sensors

Materials	Comment	$H_{\max}$ (Oe)	$\eta$ (%)	$\zeta$ (%/Oe)	Frequency (MHz)	References
$\text{Co}_{68}\text{Fe}_{4.35}\text{Si}_{12.5}\text{B}_{15}$	Conventional amorphous wire	180	1200	–	14.2	[7]
$(\text{Co}_{94}\text{Fe}_6)_{75}\text{Si}_{10}\text{B}_{15}$	Amorphous homogeneous microwire	10	125	50	3.22	[49]
$\text{Co}_{68.25}\text{Fe}_{4.5}\text{Si}_{12.25}\text{B}_{15}$	Amorphous microwire under Joule annealing	125	600	320	15	[50]
$\text{Co}_{83.2}\text{B}_{3.3}\text{Si}_{5.9}\text{Mn}_{7.6}$	Amorphous microwire under dc current	1	7.8	15.6	1	[51]
$\text{Co}_{68.2}\text{Mn}_7\text{Si}_{10}\text{B}_{15}$	Amorphous microwire	50	153	65	30	[8]
$\text{Fe}_{73.5}\text{Si}_{13.5}\text{B}_9\text{Cu}_1\text{Nb}_3$	Conventional wire annealed at 600 °C for 1 h	100	200	–	0.5	[10]
$\text{Fe}_{73.5}\text{Si}_{13.5}\text{B}_9\text{Cu}_1\text{Nb}_3$	Glass-covered microwire under conventional annealing	25	25.5	8.9	2	[19]
$\text{Fe}_{89}\text{B}_1\text{Si}_3\text{C}_3\text{Mn}_4$	Annealed at 350 °C for 1 h	300	70	–	4000	[9]
CoP/Cu/CoP electrodeposited layers	Electrodeposited technique	30	190	26	1	[24]
CoP/Cu composite wire	Electrodeposited technique	100	534	21	10.7	[39]
NiFe/Cu composite wire	Electroplated in magnetic field	45	370	47.5	1	[28]
NiFe/Cu composite wire	Joule annealing	45	1100	218	4	[41]
FeNiCo/CuBe composite wire	Electroplated technique	50	1200	–	4	[40]

(continued)

**Table 7.1** (continued)

Materials	Comment	$H_{\max}$ (Oe)	$\eta$ (%)	$\zeta$ (%/Oe)	Frequency (MHz)	References
$\text{Co}_{70}\text{Fe}_5\text{Si}_{15}\text{Nb}_{2.2}\text{Cu}_{0.8}\text{B}_7$	Ribbon under field annealing in air	2	50	125	0.1	[52]
$\text{Co}_{70}\text{Fe}_5\text{Si}_{15}\text{Nb}_{2.2}\text{Cu}_{0.8}\text{B}_7$	Ribbon under field annealing in air	2	106	35	1	[52]
$\text{Co}_{70}\text{Fe}_5\text{Si}_{15}\text{Nb}_{2.2}\text{Cu}_{0.8}\text{B}_7$	Amorphous ribbon annealed at 300 °C for 25 min	50	513	144	4	[53]
$\text{Fe}_{73.5}\text{Si}_{13.5}\text{B}_9\text{Cu}_1\text{Nb}_3$	Amorphous ribbon annealed at 550 °C for 3 h	150	400	37	4.5	[54]
$\text{Fe}_{71}\text{Al}_2\text{Si}_{14}\text{B}_{8.5}\text{Cu}_1\text{Nb}_{3.5}$	Amorphous ribbon annealed at 540 °C for 45 min	100	640	40	5	[53]
$\text{Fe}_{84}\text{Zr}_7\text{B}_8\text{Cu}_1$	Amorphous ribbon annealed at 550 °C for 1 h	75	1100	40	4.6	[55]
$\text{Fe}_{73.5}\text{Si}_{13.5}\text{B}_9\text{Cu}_1\text{Nb}_3$	Nanocrystalline sputtered film	50	80	–	500	[56]
NiFe/Au/NiFe multilayered film	RF-sputtered	65	150	30	300	[57]
NiFe/Ag multilayered film	RF-sputtered	150	250	12	18,000	[58]
FeSiBCuNb/Cu/FeSiBCuNb sandwiched film	RF-sputtered	70	1733	87	0.1	[59]
FeNiCrSiB/Cu/FeNiCrSiB sandwiched film	RF-sputtered	70	77	7.2	13	[60]
CoSiB/Cu/CoSiB sandwiched film	RF-sputtered	9	440	49	10	[61]
CoSiB/SiO <sub>2</sub> /Cu/SiO <sub>2</sub> /CoSiB sandwiched film	RF-sputtered in magnetic field	11	700	304	20	[62]
FeSiBCuNb/SiO <sub>2</sub> /Cu /SiO <sub>2</sub> /FeSiBCuNb sandwiched film	RF-sputtered	60	32	4	5.45	[63]
MuMetal alloy	Annealed at 580 °C for 40 min	115.5	310	20	0.6	[64]
Co-based amorphous ribbon/Cu/Co-based amorphous ribbon	Trilayer microstructure	20	830	–	0.28	[65]
$\text{Co}_{70.3}\text{Cr}_3\text{Fe}_{3.7}\text{B}_{10}\text{Si}_{13}$ /polymer composites	Magnetic microwires embedded in parallel in a polymer matrix	50	470	43	10	[66]

for high-performance sensor applications. In this context, the longitudinal weak-field-annealed amorphous ribbons [64, 67–74] and amorphous wires subjected to dc bias current [75–84] are promising candidate materials for producing auto-biased linear field sensors.

## References

1. Chiriac H, Ovari TA (1996) Amorphous glass-covered magnetic wires: preparation, properties, applications. *Prog Mater Sci* 40:333–407
2. Vazquez M (2001) Giant magnetoimpedance in soft magnetic “wires”. *J Magn Magn Mater* 226–230:693–699
3. Knobel M, Pirota KR (2002) Giant magnetoimpedance: concepts and recent progress. *J Magn Magn Mater* 242–245:33–40
4. Knobel M, Vazquez M, Kraus L (2003) Giant magnetoimpedance (Chap 5). In: Buschow KH (ed) *Handbook of magnetic materials*, vol 15. Elsevier Science B.V., Amsterdam, pp 1–69
5. Vazquez M, Knobel M, Sanchez ML, Valenzuela R, Zhukov AP (1997) Giant magneto-impedance effect in soft magnetic wires for sensor applications. *Sen Act A* 59:20–29
6. McHenry ME, Willard MA, Laughlin DE (1999) Amorphous and nanocrystalline materials for applications as soft magnets. *Prog Mater Sci* 44:291–433
7. Garcia D, Raposo V, Montero O, Iniguez JI (2006) Influence of magnetostriction constant on magnetoimpedance-frequency dependence. *Sen Act A* 129:227–230
8. Nie HB, Zhang XX, Pakhomov AB, Xie Z, Yan X, Zhukov A, Vazquez M (1999) Giant magnetoimpedance of glass-covered amorphous microwires of Co–Mn–Si–B and Co–Si–B. *J Appl Phys* 85:4445–4447
9. Vinai F, Coisson M, Tiberto P (2006) High-frequency magneto-impedance in metastable metallic materials: an overview. *J Magn Magn Mater* 300:e82–e87
10. Knobel M, Sanchez ML, Gomez-Polo C, Marin P, Vazquez M, Hernando A (1996) Giant magneto-impedance effect in nanostructured magnetic wires. *J Appl Phys* 79:1646–1648
11. Kraus L, Knobel M, Kane SN, Chiriac H (1999) Influence of Joule heating on magnetostriction and giant magnetoimpedance effect in a glass covered CoFeSiB microwire. *J Appl Phys* 85:5435–5437
12. Kraus L, Chiriac H, Ovari TA (2000) Magnetic properties of stress-Joule-heated amorphous FeCrBSi microwire. *J Magn Magn Mater* 215–216:343–345
13. Pirota KR, Kraus L, Chiriac H, Knobel M (2001) Magnetostriction and GMI in Joule-heated CoFeSiB glass-covered microwires. *J Magn Magn Mater* 226–230:730–732
14. Brunetti L, Tiberto P, Vinai F, Chiriac H (2001) High-frequency giant magnetoimpedance in joule-heated Co-based amorphous ribbons and wires. *Mater Sci Eng, A* 304–306:961–964
15. Li DR, Lu ZC, Zhou SX (2004) Magnetic anisotropy and stress-impedance effect in Joule heated Fe<sub>73.5</sub>Cu<sub>1</sub>Nb<sub>3</sub>Si<sub>13.5</sub>B<sub>9</sub> ribbons. *J Appl Phys* 95:204–207
16. Kurlyandskaya GV, Vazquez M, Munoz JL, Garcia D, McCord J (1999) Effect of induced magnetic anisotropy and domain structure features on magneto-impedance in stress annealed Co-rich amorphous ribbons. *J Magn Magn Mater* 196–197:259–261
17. Tejedor M, Hernando B, Sanchez ML, Prida VM, Vazquez M (1999) Stress and magnetic field dependence of magneto-impedance in amorphous Co<sub>66.3</sub>Fe<sub>3.7</sub>Si<sub>12</sub>B<sub>18</sub> ribbons. *J Magn Magn Mater* 196–197:330–332
18. Vazquez M, Hernando A (1996) A soft magnetic wire for sensor applications. *J Phys D Appl Phys* 29:939–949
19. Moron C, Garcia A (2005) Giant magneto-impedance in nanocrystalline glass-covered microwires. *J Magn Magn Mater* 290–291:1085–1088
20. Takemura Y, Tokuda H (1996) *IEEE Trans Magn* 32:4947–4949

21. Li YF, Vaquez M, Chen DX (2000) GMI effect of Fe<sub>73.5-x</sub>Cr<sub>x</sub>Cu<sub>1</sub>Nb<sub>3</sub>Si<sub>13.5</sub>B<sub>9</sub> amorphous and nanocrystalline soft wires. *J Magn Magn Mater* 249:342–345
22. Sinnecker JP, Garcia JM, Asenjo A, Vazquez M, Garcia-Arribas A (2000) Giant magnetoimpedance in CoP electrodeposited microtubes. *J Mater Res* 15:751–755
23. Yu RH, Landry G, Li YF, Basu S, Xiao JQ (2000) Magneto-impedance effect in soft magnetic tubes. *J Appl Phys* 87:4807–4809
24. Sinnecker JP, Knobel M, Pirota KR, Garcia JM, Asenjo A, Vazquez M (2000) Frequency dependence of the magnetoimpedance in amorphous CoP electrodeposited layers. *J Appl Phys* 87:4825–4827
25. Garcia JM, Sinnecker JP, Asenjo A, Vazquez M (2001) Enhanced magnetoimpedance in CoP electrodeposited microtubes. *J Magn Magn Mater* 226–230:704–706
26. Garcia JM, Asenjo A, Vazquez M, Yakunin AM, Antonov AS, Sinnecker JP (2001) Determination of closure domain penetration in electrodeposited microtubes by combined magnetic force microscopy and giant magneto-impedance techniques. *J Appl Phys* 89:3888–3891
27. Jantaratana P, Sirisathitkul C (2006) Effects of thickness and heat treatments on giant magnetoimpedance of electrodeposited cobalt on silver wires. *IEEE Trans Magn* 42:358–362
28. Li XP, Zhao ZJ, Seet HL, Heng WM, Oh TB, Lee JY (2003) Effect of magnetic field on the magnetic properties of electroplated NiFe/Cu composite wires. *J Appl Phys* 94:6655–6658
29. Li XP, Zhao ZJ, Chua C, Seet HL, Lu L (2003) Enhancement of giant magnetoimpedance effect of electroplated NiFe/Cu composite wires by dc Joule annealing. *J Appl Phys* 94:7626–7630
30. Hu J, Qin H, Zhang L, Chen J (2004) Giant magnetoimpedance effect in Ag/NiFe plate wire. *Mater Sci Eng, B* 106:202–206
31. Atalay FE, Kaya H, Atalay S (2006) Unusual grain growth in electrodeposited CoNiFe/Cu wires and their magnetoimpedance properties. *Mater Sci Eng, B* 131:242–247
32. Atalay FE, Kaya H, Atalay S (2006) Giant magnetoimpedance effect in electrodeposited CoNiFe/Cu wires with varying Ni, Fe and Co content. *J Alloys Compd* 420:9–14
33. Atalay FE, Kaya H, Atalay S (2006) Magnetoimpedance effect in electroplated NiFeRu/Cu wire. *J Phys D Appl Phys* 39:431–436
34. Velleuer J, Munoz AG, Yakabchuk H, Schiefer C, Hackl A, Kisker E (2007) Giant magnetoimpedance in electroplated NiFeMo/Cu microwires. *J Magn Magn Mater* 2:651–657
35. Zhang Z, Wu Q, Zhong K, Yang S, Lin X, Huang Z (2006) The size and space arrangement roles on coercivity of electrodeposited Co<sub>1-x</sub>Cu<sub>x</sub> nanowires. *J Magn Magn Mater* 303:e304–e307
36. Wang XZ, Yuan WZ, Zhao Z, Li XD, Ruan JZ, Yang XL (2005) Giant magnetoimpedance effect in CuBe/NiFeB and CuBe/insulator/NiFeB electroless-deposited composite wires. *IEEE Trans Magn* 41:113–115
37. Wang XZ, Yuan WZ, Zhao Z, Li XD, Ruan JZ, Zhao ZJ, Yang JX, Yang XL, Sun Z (2007) Enhancement of giant magnetoimpedance in composite wire with insulator layer. *J Magn Magn Mater* 308:269–272
38. Usov N, Antonov A, Granovsky A (1997) Theory of giant magnetoimpedance effect in composite amorphous wire. *J Magn Magn Mater* 171:64–68
39. Phan MH, Peng HX, Wisnom MR, Tung MT, Dung NV, Nghi NH (2007) Optimized GMI effect in electrodeposited CoP/Cu composite wires. *J Magn Magn Mater* 2:244–247
40. Kurlyandskays GV, Garcia-Arribas A, Barandiaran JM (2003) Advantages of nonlinear giant magnetoimpedance for sensor applications. *Sens Actuators A* 106:234–239
41. Li XP, Seet HL, Fran J, Yi JB (2006) Electrodeposition and characteristics of Ni<sub>80</sub>Fe<sub>20</sub>/Cu composite wires. *J Magn Magn Mater* 304:111–116
42. Buznikov NA, Antonov AS, Granovsky AB, Kim CG, Kim CO, Li XP, Yoon SS (2006) Giant magnetoimpedance in composite wires with insulator layer between non-magnetic core and soft magnetic shell. *J Magn Magn Mater* 300:e63–e66

43. Pirola K, Hernandez-Velez M, Navas D, Zhukov A, Vázquez M (2004) Multilayer microwires: tailoring magnetic behavior by sputtering and electroplating. *Adv Funct Mat* 14:266–268
44. Pirola K, Provencio M, García K, Hernandez-Velez M, Vázquez MJ (2005) *Magn Magn Mat* 290–291:68
45. Vázquez M, Pirola K, Torrejon J, Badini G, Torcunov AJ (2006) *Magn Magn Mater* 304: 197–202
46. Torrejón J, Badini G, Pirola K, Vázquez M (2007) *Acta Mater* 55:4271–4276
47. Vazquez M (2007) Advanced magnetic microwires. In: Kronmüller H, Parkin S (ed) *Handbook of magnetism and advanced magnetic materials*. Wiley&Sons, NJ
48. Torrejón J, Infante G, Badini-Confalonieri G et al (2013) *J Miner Met Mater Soc* 65(7): 890–900
49. Vazquez M, Garcia-Beneytez JM, Garcia JM, Sinnecker JP, Zhukov AP (2000) Giant magneto-impedance in heterogeneous microwires. *J Appl Phys* 88:6501–6505
50. Pirola KR, Kraus L, Chiriac H, Knobel M (2000) Magnetic properties and giant magnetoimpedance in a CoFeSiB glass-covered microwire. *J Magn Magn Mater* 221: L243–L247
51. Phan MH, Yu SC, Kim CG, Vazquez M (2003) Origin of asymmetrical magnetoimpedance in a Co-based amorphous microwire due to dc bias current. *Appl Phys Lett* 83:2871–2873
52. Phan MH, Peng HX, Yu SC, Chau N (2005) Valve behavior of giant magnetoimpedance in field-annealed  $\text{Co}_{70}\text{Fe}_5\text{Si}_{15}\text{Nb}_{2.2}\text{Cu}_{0.8}\text{B}_7$  amorphous ribbon. *J Appl Phys* 97:10M108, 1–3
53. Phan MH, Peng HX, Yu SC, Vazquez M (2006) Optimized giant magnetoimpedance effect in amorphous and nanocrystalline materials. *J Appl Phys* 99:08C505, 1–3
54. Guo HQ, Kronmuller H, Dragon T, Cheng ZH, Shen BG (2001) Influence of nanocrystallization on the evolution of domain patterns and the magnetoimpedance effect in amorphous  $\text{Fe}_{73.5}\text{Cu}_1\text{Nb}_3\text{Si}_{13.5}\text{B}_9$  ribbons. *J Appl Phys* 89:514–516
55. Lee HB, Kim KJ, Kim TK, Kim CO, Yu SC (2000) Magnetoimpedance effect in the nanocrystalline Fe–Zr–Cu–B–Al alloy system. *J Appl Phys* 87:5269–5291
56. Viegas ADC, de Andrade AMH, Sommer RL, Jiang JS, Chien CL (2001) Magnetoimpedance in  $\text{Fe}_{73.5}\text{Cu}_1\text{Nb}_3\text{Si}_{13.5}\text{B}_9$  amorphous films at microwave frequencies. *J Magn Magn Mater* 226–230:707–708
57. de Cos D, Fry N, Orue I, Panina PV, Garcia-Arribas A, Barandiaran JM (2006) Very large magnetoimpedance (MI) in FeNi/Au multilayer film systems. *Sens Actuators A* 129:256–259
58. de Andrade AMH, da Silva RB, Correa MA, Viegas ADC, Severino AM, Sommer RL (2004) Magnetoimpedance of NiFe/Ag multilayers in the 100 kHz–1.8 GHz range. *J Magn Magn Mater* 272–276:1846–1847
59. Xiao SQ, Liu YH, Yan SS, Dai YY, Zhang L, Mei LM (2000) Giant magnetoimpedance and domain structure in FeCuNbSiB films and sandwiched films. *Phys Rev B* 61:5734–5739
60. Xiao SQ, Liu YH, Dai YY, Zhang L, Zhou SX, Liu GD (1999) Giant magnetoimpedance effect in sandwiched films. *J Appl Phys* 85:4127–4130
61. Morikawa T, Nishibe Y, Yamadera H (1997) Giant magnetoimpedance effect in layered thin films. *IEEE Trans Magn* 33:4367–4372
62. Morikawa T, Nishibe Y, Yamadera H, Nonomura Y, Takeuchi M, Sakata J, Taga Y (1996) Enhancement of giant magneto-impedance in layered film by insulator separation. *IEEE Trans Magn* 32:4965–4967
63. Li XD, Yuan WZ, Zhao ZJ, Ruan JZ, Yang XL (2005) The GMI effect in nanocrystalline FeCuNbSiB multilayered films with a  $\text{SiO}_2$  outer layer. *J Phys D Appl Phys* 38:1351–1354
64. Nie HB, Pakhomov AB, Yan X, Zhang XX, Knobel M (1999) Giant magnetoimpedance in crystalline Mumetal. *Sol Stat Commn* 112:285–289
65. Amalou F, Gijis MAM (2004) Giant magnetoimpedance of amorphous ribbon/Cu/amorphous ribbon trilayer microstructures. *J Appl Phys* 95:1364–1371
66. Phan MH, Peng HX, Wisnom MR, Yu SC, Nghi NH Great enhancement of GMI effect in polymer composites containing Co-based ferromagnetic microwires. *J Magn Magn Mater* (in press)

67. Fu CM, Hsu CY, Chao YC, Kim DS, Matsushita N, Abe M (2004) Tunnel magnetoimpedance effect of the ZnNi-ferrite encapsulated NiFe micropsheres. *J Magn Magn Mater* 272–276: e1839–e1841
68. Hu J, Qin H, Qi G, Jiang M (2006) Giant magnetoimpedance in a MnZn ferrite. *J Magn Magn Mater* 302:375–377
69. Carara M, Sommer RL (1997) Giant magnetoimpedance in highly textured (110)[001] FeSi<sub>3</sub> %. *J Appl Phys* 81:4107–4109
70. Gomez-Polo C, Perez-Landazabal JI, Recarte V, Ciurzynska W (2003) Effect of the ordering on the magnetic and magnetoimpedance properties of Fe-6.5 % Si alloy. *J Magn Magn Mater* 254–255:88–90
71. Jantaratana P, Sirisathitkul C (2004) Giant magnetoimpedance in silicon steels. *J Magn Magn Mater* 281:399–404
72. Hu J, Qin H (2002) Magnetoimpedance effect in Fe flakes. *J Magn Magn Mater* 246:375–378
73. Soares JM, de Araujo JH, Cabral FAO, Dumelow T, Machado FLA, de Araujo AEP (2002) Giant magnetoimpedance in FeAg granular alloys. *Appl Phys Lett* 80:2532–2534
74. Fraga GLF, Pureur P, Brandao DE (2002) Spontaneous magnetoimpedance in the Heusler compounds Pd<sub>2</sub>MnSn and Pd<sub>2</sub>MnSb near the Curie temperature. *Sol Stat Comm* 124:7–10
75. Fu CM, Hsu KS, Lin ML, Wen ZH (2000) Giant magnetoimpedance effects in sintered La<sub>1-x</sub>Ca<sub>x</sub>MnO<sub>3</sub> oxides. *J Magn Magn Mater* 209:151–153
76. Hu J, Qin HW (2003) Magnetoimpedance effect at various temperatures for manganite La<sub>0.7</sub>Ca<sub>0.3</sub>MnO<sub>3-σ</sub>. *Mater Sci Eng B* 100:304–306
77. Castro GMB, Rodrigues AR, Machado FLA, de Araujo AEP, Jardim RF, Nigam AK (2004) Magnetoimpedance measurements in bulk samples of La<sub>0.7</sub>Ca<sub>0.3</sub>MnO<sub>3</sub> and La<sub>0.6</sub>Y<sub>0.1</sub>Ca<sub>0.3</sub>MnO<sub>3</sub>. *J All Comp* 369:108–111
78. Hu J, Qin HW (2001) Magnetoimpedance effect in La<sub>0.7</sub>Sr<sub>0.3</sub>MnO<sub>3</sub>. *J Magn Magn Mater* 234:419–422
79. Hu J, Qin HW (2001) Giant magnetoimpedance effect in La<sub>0.65</sub>Sr<sub>0.35</sub>MnO<sub>3</sub> under low dc magnetic fields. *Mater Sci Eng B* 79:186–189
80. Hu J, Qin HW (2002) Magnetoimpedance effect in semiconducting La<sub>0.4</sub>Sr<sub>0.6</sub>MnO<sub>3</sub>. *Mater Sci Eng B* 88:18–21
81. Patanjali PV, Theule P, Zhai Z, Hakim N, Sridhar S, Suryanarayanan R, Apostu M, Dhahenne G, Revcolevschi A (1999) High-frequency magnetoimpedance of double perovskite La<sub>1.2</sub>Sr<sub>1.8</sub>Mn<sub>2</sub>O<sub>7</sub>: secondary transitions at high temperatures. *Phys Rev B* 60:9268–9271
82. Hu J, Qin HW, Zhang Y (2000) Giant magnetoimpedance effect in La–Ba–Mn–O oxide. *Mater Sci Eng B* 77:280–281
83. Hu J, Qin HW (2000) Magnetoimpedance effect in La<sub>0.67</sub>Ba<sub>0.33</sub>MnO<sub>3</sub> under low dc magnetic fields. *Sol Stat Commun* 116:159–162
84. Hu J, Qin HW, Niu HD, Zhu L, Chen J, Xiao W, Pei Y (2003) Magnetoimpedance effect in manganite La<sub>2/3</sub>Ba<sub>1/3</sub>MnO<sub>3</sub> at various temperatures. *J Magn Magn Mater* 261:105–111